

High-order/*hp*-adaptive discontinuous Galerkin finite element methods for acoustic problems.

Stefano Giani

Abstract In this paper we present two different kinds of error estimators for acoustic problems: a residual-based and a dual weighted residual one. The former error estimator is explicit and cheap to compute. The latter is based on a duality argument and it is capable of computing accurate and reliable estimations of quantities of interest, which can be safely used for finite element analysis and model validation. The error estimators presented in this work are designed to work with a *hp*-adaptive discontinuous Galerkin (DG) methods.

Keywords finite element method · *hp*-adaptivity · a posteriori error estimates · acoustics

Mathematics Subject Classification (2000) 65N30 · 65N50 · 65N15

1 Introduction

In the last decades the internal noise of road vehicles has been of increasing interest to manufacturers and customers. It is particularly important that manufacturers are able to predict the noise at an early stage of a new design so that expensive mistakes can be avoided. There are several numerical methods that can be used (see [1] for an overview) and new methods continue to appear. One of the most common is wave-based modelling method [2–7] where the domain is subdivided into a number of convex subdomains and a set of wave functions for each sub-domain is selected to construct the system matrices.

Moreover other methods of completely different nature are also available like statistical energy analysis (SEA) and ray tracing methods, in between them we can find dynamical energy analysis (DEA) methods [8–10] which interpolate between the two of them. DEA methods are particularly interesting because SEA and ray tracing are in fact complementary in many ways. Ray

S. Giani
School of Mathematical Sciences, University of Nottingham, University Park, Nottingham,
NG7 2RD, UK. E-mail: stefanogiani79@gmail.com

tracing handles wave problems with a small number of reflections very well. On the other hand SEA is suitable for complex structures carrying wave energy over many sub-elements including potentially a large number of reflections and scattering events.

Another class of methods consists in those based on finite element methods (FEMs). This kind of methods seems to be the most accurate according to [1] and they come in a big variety: there are both polynomial based methods [11, 12] and non-polynomial based methods [13–16].

Adaptivity can be used with FEMs to improve the accuracy of numerical solutions with a modest increase in the computational costs. There are mainly two ways to adapt elements in a mesh, by splitting the elements in smaller elements - h -adaptivity - or by changing order of polynomials used in the elements - p -adaptivity. However, by far the most efficient adaptive technique is called hp -adaptivity which embraces both ways deciding for each element which of the two techniques to apply. In order to adapt a mesh to improve the accuracy of the computed solution it is necessary first of all to understand the distribution of the error across the mesh. This very delicate task is normally accomplished using error estimators. In this paper we present two different kinds of error estimators for acoustic problems: a residual-based and a dual weighted residual (DWR) one. The former error estimator is explicit and cheap to compute. The latter is based on a duality argument and it is capable of computing accurate and reliable estimations of quantities of interest. With minor modifications, the error estimators presented in this paper can be used with continuous Galerkin methods as well.

In this paper we are going to consider the source model problem (1), which can be used to simulate the behavior of an acoustic system under the action of an external force. Equation (1) is the complex valued formulation of the Helmholtz's equation in a bounded and either polygonal or polyhedral domain Ω contained in \mathbb{R}^d , where $d = 2, 3$. To make the exposition simple we allow only for Dirichlet boundary conditions on $\partial\Omega$.

$$\begin{cases} -\nabla \cdot (\mathcal{A}\nabla u) - (\omega/c)^2 u = f & \text{in } \Omega, \\ u = p & \text{on } \partial\Omega. \end{cases} \quad (1)$$

Moreover we denote by f the external force, by ω the frequency and by $c > 0$ the speed of sound. We allow for ω to be complex in order to introduce damping into the model. The boundary conditions are characterized by the complex valued function $p \in H^{1/2}(\partial\Omega)$. The remaining coefficient \mathcal{A} may be discontinuous and it can be used to model the presence of different materials with different densities in the system, we assume that the matrix-valued function \mathcal{A} is real symmetric and uniformly positive definite, i.e.

$$0 < \underline{a} \leq \xi^T \mathcal{A}(x) \xi \leq \bar{a} \quad \text{for all } \xi \in \mathbb{R}^2 \quad \text{with } |\xi| = 1 \quad \text{and all } x \in \Omega. \quad (2)$$

The paper is structured as follows: In Section 2 we provide a detailed description of the hp -DG weak formulation of our model problem. Section 3 provides the background and basic results for the energy norm error estimator.

Section 4 provides the background and basic results for the DWR error estimator. We describe our adaptive procedure in Section 5. Section 6, is devoted to presenting and discussing the numerical results.

2 Formulation of the discontinuous Galerkin method

Throughout $L^2(\Omega)$ denotes the usual space of square integrable complex valued functions equipped with the standard norm. When we want to restrict this norm to a measurable subset $S \subseteq \Omega$, we write $\|g\|_{0,S}$, etc.

Since we are going to construct sequences of adaptively refined shape-regular meshes with at most one hanging node per face, we denote the meshes by \mathcal{T}_n , where n is the index of the mesh. The meshes \mathcal{T}_n are either partitions of $\Omega \subset \mathbb{R}^2$ into open triangles or quadrilaterals $\{K\}_{K \in \mathcal{T}_n}$ or partitions of $\Omega \subset \mathbb{R}^3$ into open tetrahedrons or hexahedrons. We also assume that, in the interior of each element $K \in \mathcal{T}_n$, the positive definite matrix \mathcal{A} is constant. In presence of jumping coefficients, the jumps are aligned with the meshes used in this work. The diameter of an element $K \in \mathcal{T}_n$ is denoted by h_K . Furthermore, we assume that these diameters are of bounded variation, i.e. there is a constant $b_1 \geq 1$ such that

$$b_1^{-1} \leq h_K/h_{K'} \leq b_1, \quad (3)$$

whenever K and K' share a common face. We store the diameters of the elements of \mathcal{T}_n in the mesh size vector $\mathbf{h} = (h_K)_{K \in \mathcal{T}_n}$. Similarly, we associate with each element $K \in \mathcal{T}_n$ a polynomial degree $p_K \geq 1$ and define the degree vector $\mathbf{p} = (p_K)_{K \in \mathcal{T}_n}$. We assume that \mathbf{p} is of bounded variation as well, i.e. there is a constant $b_2 \geq 1$ such that

$$b_2^{-1} \leq p_K/p_{K'} \leq b_2, \quad (4)$$

whenever K and K' share a common face.

For a partition \mathcal{T}_n of Ω and a degree vector \mathbf{p} , we define the discontinuous Galerkin (DG) finite element space S_n of complex valued functions by

$$S_n = \{v \in L^2(\Omega) : v|_K \in \mathcal{P}_{p_K}(K), K \in \mathcal{T}_n\}, \quad (5)$$

where, if K is either a triangular or a tetrahedral element, $\mathcal{P}_{p_K}(K)$ is the space of polynomials on K of total degree less or equal to p_K , otherwise if K is either a quadrilateral or a brick element, $\mathcal{P}_{p_K}(K)$ is the space of polynomials on K of degree less or equal to p_K in each dimension.

Next, we define some trace operators that are required for the DG method. To this end, we denote by $\mathcal{E}_{\mathcal{T},n}$ the set of all interior faces of the partition \mathcal{T}_n of Ω , and by $\mathcal{E}_{\Gamma,n}$ the set of all boundary faces of \mathcal{T}_n . Furthermore, we define $\mathcal{E}_n = \mathcal{E}_{\mathcal{T},n} \cup \mathcal{E}_{\Gamma,n}$. The boundary ∂K of an element K and the sets $\partial K \setminus \Gamma$ and $\partial K \cap \Gamma$ will be identified in a natural way with the corresponding subsets of \mathcal{E}_n .

Let K^+ and K^- be two adjacent elements of \mathcal{T}_n , and $e \in \mathcal{E}_{\mathcal{T},n}$ be given by $e = \partial K^+ \cap \partial K^-$. Furthermore, let v be a scalar-valued function, that is

smooth inside each element K^\pm . By v^\pm , we denote the traces of v on e taken from within the interior of K^\pm , respectively. Since we are dealing with jumping coefficients we use the definition of the weighted average of the diffusive flux from [17]. Following the definition in [17] we define the diffusive flux $\mathcal{A}\nabla_n v$ along $e \in \mathcal{E}_{\mathcal{I},n}$ as:

$$\{\{\mathcal{A}\nabla_n v\}\} = \omega^- (\mathcal{A}\nabla_n v)^- + \omega^+ (\mathcal{A}\nabla_n v)^+ ,$$

where

$$\omega^- = \frac{\mathbf{n}_{K^+}^T \mathcal{A}^+ \mathbf{n}_{K^+}}{\mathbf{n}_{K^-}^T \mathcal{A}^- \mathbf{n}_{K^-} + \mathbf{n}_{K^+}^T \mathcal{A}^+ \mathbf{n}_{K^+}} , \quad \omega^+ = \frac{\mathbf{n}_{K^-}^T \mathcal{A}^- \mathbf{n}_{K^-}}{\mathbf{n}_{K^-}^T \mathcal{A}^- \mathbf{n}_{K^-} + \mathbf{n}_{K^+}^T \mathcal{A}^+ \mathbf{n}_{K^+}} ,$$

where we denote by \mathbf{n}_{K^\pm} the unit outward normal vector of ∂K^\pm , respectively. Similarly, for a scalar function we have the following weighted average

$$\{\{v\}\} = \omega^- v^+ + \omega^+ v^- .$$

Then, the jump of v across $e \in \mathcal{E}_{\mathcal{I}}(\mathcal{T}_n)$ is given by

$$\llbracket v \rrbracket = v^+ \mathbf{n}_{K^+} + v^- \mathbf{n}_{K^-} ,$$

$$\llbracket \mathcal{A}\nabla_n v \rrbracket = \mathcal{A}^+ \nabla_n v^+ \cdot \mathbf{n}_{K^+} + \mathcal{A}^- \nabla_n v^- \cdot \mathbf{n}_{K^-} .$$

On a boundary face $e \in \mathcal{E}_{\Gamma,n}$, we set $\{\{\mathcal{A}\nabla_n v\}\} = \mathcal{A}\nabla_n v$ and $\llbracket v \rrbracket = \mathbf{v}\mathbf{n}$, with \mathbf{n} denoting the unit outward normal vector on the boundary Γ .

Remark 1 The weighted mean value $\{\{\cdot\}\}$ satisfies the following relation:

$$(\mathcal{A}\nabla_n u)^+ \cdot \mathbf{n}_{K^+} v^+ + (\mathcal{A}\nabla_n u)^- \cdot \mathbf{n}_{K^-} v^- = \{\{\mathcal{A}\nabla_n u\}\} \cdot \llbracket v \rrbracket + \llbracket \mathcal{A}\nabla_n u \rrbracket \cdot \{\{v\}\} , \quad (6)$$

which is already a well-known result for the standard DG mean value [18].

For a mesh \mathcal{T}_n on Ω and a polynomial degree vector \mathbf{p} , let S_n be the finite element space defined in (5). We consider the (symmetric) weighted interior penalty discretization [17] of (1): find $u_n \in S_n$ such that

$$A_n(u_n, v) = F(v) , \quad \text{for all } v \in S_n , \quad (7)$$

where

$$\begin{aligned} A_n(u, v) &:= \sum_{K \in \mathcal{T}_n} \int_K \mathcal{A}_K \nabla_n u \cdot \nabla_n \bar{v} - (\omega/c)^2 u \bar{v} dx \\ &\quad - \sum_{e \in \mathcal{E}_n} \int_e (\{\{\mathcal{A}\nabla_n \bar{v}\}\} \cdot \llbracket u \rrbracket + \{\{\mathcal{A}\nabla_n u\}\} \cdot \llbracket \bar{v} \rrbracket) ds + \sum_{e \in \mathcal{E}_n} \int_e c \llbracket u \rrbracket \cdot \llbracket \bar{v} \rrbracket ds , \\ F(v) &:= \sum_{K \in \mathcal{T}_n} \int_K f \bar{v} dx - \sum_{e \in \mathcal{E}_{\Gamma,n}} \int_e p \mathbf{n} \cdot \nabla_n \bar{v} ds + \sum_{e \in \mathcal{E}_{\Gamma,n}} \int_e c p \bar{v} ds . \end{aligned}$$

here, ∇_n denotes the element-wise gradient operator and \mathcal{A}_K denotes the restriction of \mathcal{A} onto K . Furthermore, the function $\mathbf{c} \in L^\infty(\mathcal{E}_n)$ is the discontinuity stabilization function that is chosen as follows: we define the functions $\mathbf{h} \in L^\infty(\mathcal{E}_n)$ and $\mathbf{p} \in L^\infty(\mathcal{E}_n)$ by

$$\mathbf{h}(\mathbf{r}) := \begin{cases} \min(h_{K^+}, h_{K^-}), & \mathbf{r} \in e \in \mathcal{E}_{\mathcal{I},n}, e = \partial K^+ \cap \partial K^-, \\ h_K, & \mathbf{r} \in e \in \mathcal{E}_{\Gamma,n}, e \in \partial K \cap \Gamma, \end{cases}$$

$$\mathbf{p}(\mathbf{r}) := \begin{cases} \max(p_{K^+}, p_{K^-}), & \mathbf{r} \in e \in \mathcal{E}_{\mathcal{I},n}, e = \partial K^+ \cap \partial K^-, \\ p_K, & \mathbf{r} \in e \in \mathcal{E}_{\Gamma,n}, e \in \partial K \cap \Gamma, \end{cases}$$

and set the penalty parameter to be

$$\mathbf{c} = \alpha \gamma_K \frac{\mathbf{p}^2}{\mathbf{h}}, \quad (8)$$

with $\gamma_K = \omega^+ \mathbf{n}_{K^+}^T \mathcal{A}^+ \mathbf{n}_{K^+} = \omega^- \mathbf{n}_{K^-}^T \mathcal{A}^- \mathbf{n}_{K^-}$, and with a parameter $\alpha > 0$ that is independent of \mathbf{h} , \mathbf{p} , \mathcal{A}^+ and \mathcal{A}^- . The parameter \mathbf{c} defined here is an hp -version of the weighted penalty parameter [17].

3 Energy norm a posteriori error estimator

An a posteriori error estimator is an essential part of the adaptive procedure, since it determines where it is necessary to adapt the mesh and the finite element space to minimize the error of the computed solution. This is possible because the a posteriori error estimator is capable of estimating the error in each element from the computed solution u_n .

The main results in this section are theorems 1 and 2 showing the reliability and the efficiency of the residual error estimator introduced below. The reliability ensures that, up to a constant and to asymptotically higher order terms, the error estimator η_j gives rise to an a posteriori upper bound for error in the energy norm; on the other hand, the efficiency ensures that, up to a constant and to asymptotically higher order terms, the true error bounds the error estimator η_j from above. Together these two results ensure that the computable quantity η_j is linearly proportional to the true error, up to asymptotically higher order terms. So it is safe to assume that the true error decays on a sequence of meshes where the a posteriori error η_j decays, too.

In this section we are going to extend the results from [19] to acoustic problems with discontinuous coefficients. The results from [19] cannot be applied straightaway in this case because the presence of the term $-(\omega/c)^2 u$ in (1) is making the problem non-coercive. Similarly to [19] the error estimator η is defined as:

$$\eta^2 := \sum_{K \in \mathcal{T}_n} \eta_K^2,$$

where η_K is the estimation of the error on the element K . The terms η_K are defined as follows:

$$\eta_K^2 := \eta_{R_K}^2 + \eta_{F_K}^2 + \eta_{J_K}^2 ,$$

where

$$\eta_{R_K}^2 := p_K^{-2} h_K^2 \|f_n + \nabla \cdot (\mathcal{A} \nabla u_n) + (\omega/c)^2 u_n\|_{0,K}^2 ,$$

$$\eta_{F_K}^2 := \frac{1}{2} \sum_{e \in \mathcal{E}_{I,n}} p_e^{-1} h_e \|[\![\mathcal{A} \nabla u_n]\!] \|_{0,e}^2 ,$$

$$\eta_{J_K}^2 := \frac{1}{2} \sum_{e \in \mathcal{E}_{I,n}} c \| [u_n] \|_{0,e}^2 + \sum_{e \in \mathcal{E}_{\Gamma,n}} c \| u_n - p_n \|_{0,e}^2 ,$$

where p_n is the trace of a function in $H^1(\Omega)$ such that

$$p_n|_e \in \mathcal{P}_{p_K}(e), \quad e \in \mathcal{E}_{\Gamma,n}, e \in \partial K \cap \partial \Omega, K \in \mathcal{T}_n,$$

and where f_n is the elementwise L^2 projection of f onto the finite element space.

In order to extend the theory in [19] we need to introduce an auxiliary coercive problem. Consider the following problem related to (1):

$$\begin{cases} -\nabla \cdot (\mathcal{A} \nabla \hat{u}) = g & \text{in } \Omega, \\ \hat{u} = p & \text{on } \partial \Omega, \end{cases} \quad (9)$$

with $g \in L^2(\Omega)$ and the corresponding DG formulation: find $\hat{u}_n \in S_n$ such that

$$B_n(\hat{u}_n, v) = G(v), \quad \text{for all } v \in S_n, \quad (10)$$

where

$$\begin{aligned} B_n(\hat{u}, v) &:= \sum_{K \in \mathcal{T}_n} \int_K \mathcal{A}_K \nabla_n \hat{u} \cdot \nabla_n \bar{v} \, dx \\ &\quad - \sum_{e \in \mathcal{E}_n} \int_e (\{ \mathcal{A} \nabla_n \bar{v} \} \cdot [\![\hat{u}]\!] + \{ \mathcal{A} \nabla_n \hat{u} \} \cdot [\![\bar{v}]\!]) \, ds + \sum_{e \in \mathcal{E}_n} \int_e c [\![\hat{u}]\!] \cdot [\![\bar{v}]\!] \, ds, \\ G(v) &:= \sum_{K \in \mathcal{T}_n} \int_K g_n \bar{v} \, dx - \sum_{e \in \mathcal{E}_{\Gamma,n}} \int_e p \, n \cdot \nabla_n \bar{v} \, ds + \sum_{e \in \mathcal{E}_{\Gamma,n}} \int_e c p \bar{v} \, ds, \end{aligned}$$

where g_n is some approximation of g onto the finite element space.

As for problem (1), we define an error estimator also for problem (9):

$$\hat{\eta}^2 := \sum_{K \in \mathcal{T}_n} \hat{\eta}_K^2 ,$$

where $\hat{\eta}_K$ is the estimation of the error on the element K . The terms $\hat{\eta}_K$ are defined as follows:

$$\hat{\eta}_K^2 := \hat{\eta}_{R_K}^2 + \hat{\eta}_{F_K}^2 + \hat{\eta}_{J_K}^2 ,$$

where

$$\hat{\eta}_{R_K}^2 := p_K^{-2} h_K^2 \|g_n + \nabla \cdot (\mathcal{A} \nabla \hat{u}_n)\|_{0,K}^2 ,$$

$$\hat{\eta}_{F_K}^2 := \frac{1}{2} \sum_{e \in \mathcal{E}_{I,n}} p_e^{-1} h_e \|\llbracket \mathcal{A} \nabla \hat{u}_n \rrbracket\|_{0,e}^2 ,$$

$$\hat{\eta}_{J_K}^2 := \frac{1}{2} \sum_{e \in \mathcal{E}_{I,n}} c \|\llbracket \hat{u}_n \rrbracket\|_{0,e}^2 + \sum_{e \in \mathcal{E}_{\Gamma,n}} c \|\hat{u}_n - p_n\|_{0,e}^2 ,$$

Lemma 1 *Let \hat{u} be the solution of (9) and $\hat{u}_n \in S_n$ its DG approximation obtained by (10). Then we have that the error in the norm*

$$\|\hat{u}\|_{DG, \mathcal{T}_n}^2 := \sum_{K \in \mathcal{T}_n} \|\mathcal{A} \nabla \hat{u}\|_{0,K}^2 + \sum_{e \in \mathcal{E}_n} c \|\llbracket \hat{u} \rrbracket\|_{0,e}^2 , \quad (11)$$

is bounded by $\hat{\eta}$ multiplied by a hidden constant independent of h and p , i.e.

$$\|\hat{u} - \hat{u}_n\|_{DG, \mathcal{T}_n} \lesssim \hat{\eta} + \hat{\Theta} , \quad (12)$$

where the term $\hat{\Theta}$ is a higher order term defined as:

$$\hat{\Theta}^2 := \sum_{K \in \mathcal{T}_n} p_K^{-2} h_K^2 \|g - g_n\|_{0,K}^2 + \|p - p_n\|_{1/2, \partial\Omega}^2 + \sum_{e \in \mathcal{E}_{\Gamma,n}} c \|p - p_n\|_{0,e}^2 .$$

The proof of this lemma is equivalent to the proof of Theorem 3.1 in [19].

Lemma 2 *Let \hat{u} be the solution of (9) and $\hat{u}_n \in S_n$ its DG approximation obtained by (10). Then we have the local upper bound*

$$\eta \lesssim \|\hat{u} - \hat{u}_n\|_{DG, \mathcal{T}_n} + \Theta .$$

The proof of this lemma is equivalent to the proof of Corollary 3.1 in [19] with $\alpha = 0$.

Now, choosing $g := f + (\omega/c)^2 u$, we have that $u \equiv \hat{u}$ and similarly choosing $g_n := f_n + (\omega/c)^2 u_n$, we have that $u_n \equiv \hat{u}_n$ and that $\eta \equiv \hat{\eta}$. So using Lemma 1 and Lemma 2 we have the following two theorems which show the reliability and efficiency of the error estimator for problem (1).

Theorem 1 (Reliability) *Let u be the solution of (1) and $u_n \in S_n$ its DG approximation obtained by (7). Then we have that the error is bounded by η multiplied by a hidden constant independent of h and p , i.e.*

$$\|u - u_n\|_{DG, \mathcal{T}_n} \lesssim \eta + \Theta , \quad (13)$$

where the term Θ is as:

$$\Theta^2 := \sum_{K \in \mathcal{T}_n} p_K^{-2} h_K^2 \|f - f_n\|_{0,K}^2 + \sum_{K \in \mathcal{T}_n} p_K^{-2} h_K^2 (\omega/c)^2 \|u - u_n\|_{0,K}^2$$

$$+ \|p - p_n\|_{1/2, \partial\Omega}^2 + \sum_{e \in \mathcal{E}_{\Gamma,n}} c \|p - p_n\|_{0,e}^2 .$$

Proof From Lemma 1 and recalling that $g := f + (\omega/c)^2 u$ and $g_n := f_n + (\omega/c)^2 u_n$, we have

$$\|u - u_n\|_{DG, \mathcal{T}_n} = \|\hat{u} - \hat{u}_n\|_{DG, \mathcal{T}_n} \lesssim \hat{\eta} + \hat{\Theta} \leq \eta + \Theta .$$

All the terms Θ^2 with the exception of $\sum_{K \in \mathcal{T}_n} p_K^{-2} h_K^2 (\omega/c)^2 \|u - u_n\|_{0,K}^2$ are higher order terms compared to $\|u - u_n\|_{DG, \mathcal{T}_n}$ and they are unlikely to become dominant. In general the L^2 norm of the error is asymptotically of higher order compared to the DG norm of the error, however in our case for big enough values of ω , the term $\sum_{K \in \mathcal{T}_n} p_K^{-2} h_K^2 (\omega/c)^2 \|u - u_n\|_{0,K}^2$ can become dominant especially on coarse meshes. Nevertheless in the first example presented in Section 6 the error estimator η mimics very well the behavior of the DG error even if ω has a quite big value, suggesting that even in case that Θ is dominant, the error estimator continues to predict correctly the distribution of the error.

Theorem 2 (Efficiency) *Let u be the solution of (1) and $u_n \in S_n$ its DG approximation obtained by (7). Then we have the local upper bound*

$$\eta \lesssim \|u - u_n\|_{DG, \mathcal{T}_n} + \Theta .$$

Proof From Lemma 2 and recalling that $g := f + (\omega/c)^2 u$ and $g_n := f_n + (\omega/c)^2 u_n$, we have

$$\eta = \hat{\eta} \lesssim \|\hat{u} - \hat{u}_n\|_{DG, \mathcal{T}_n} + \hat{\Theta} \leq \|u - u_n\|_{DG, \mathcal{T}_n} + \Theta .$$

4 Dual weighted residual a posteriori error estimator

The main two drawbacks of the energy norm a posteriori error estimator η are firstly the presence of the hidden constants, which makes η an estimator of the error and not an approximation of the error. In fact even if the true error and η are asymptotically linked together, their values could be very far apart. The second drawback is that the only estimated measurement of the error that η can provide is the DG norm in (11) of the error and so the sequence of obtained meshes are constructed to minimize only such norm. However, very often in practice people are interested in different measurements of the error for example in acoustics the error of the computed solution in a specific point in the domain, where a sensor may sit, could be of great interest.

To compensate for all these drawbacks, it is advisable to use a more advanced a posteriori error estimator called dual weighted residual (DWR) a posteriori error estimator [20, 21]. The main characteristic of this type of error estimator is the fact that the measurement of the error to target with the adaptive process can be easily changed. Commonly the measurement of the error that are used with DWR are quantities with physical meaning. In this way a DWR adaptive algorithm can be used to accurately estimate specific quantities for practical interest. For this reason DWR has been already used in many fields. For example in [22] DWR has been used to accurately compute the lift and drag of wing profile, moreover in [23, 24] DWR has been used to

accurately compute eigenvalues of eigenvalue problems from different areas of physics.

The main difference between DWR and the error estimator presented in the previous section is that in order to compute the residuals of the DWR error estimator, it is necessary to compute the solution of an auxiliary problem which is related to the dual/adjoint operator in (7) and whose definition depends on the choice of the measurement of the solution to target. Let us assume that the quantity to target can be expressed as a linear functional $J(\cdot)$. Such functional is used in the definition of the auxiliary problem, that implies that the solution z of the auxiliary problem depends on the definition of $J(\cdot)$. In conclusion, the mechanism that makes DWR very flexible and able to target easily different quantities of interest is the fact that the residual is computed using z , which is linked to the definition of $J(\cdot)$. So a different choice of $J(\cdot)$ will lead to a different solution z to be used in the residuals and a different behavior of the adaptive strategy.

Let us introduce the variational formulation of problem (1):

$$A(u, v) := \int_{\Omega} \mathcal{A} \nabla u \cdot \nabla \bar{v} - (\omega/c)^2 u \bar{v} dx = \int_{\Omega} f \bar{v} dx =: F_c(v), \quad (14)$$

where the test functions $v \in H_{\Gamma}^1(\Omega)$, which is the subspace of $H^1(\Omega)$ of functions with null trace along Γ . Moreover u should be found in $H_g^1(\Omega)$, which is the subspace of $H^1(\Omega)$ of functions with trace equal to g along Γ . Similarly we define the dual problem of (1) as

$$A(w, z) = J(w), \quad (15)$$

with $w \in H_g^1(\Omega)$ and $z \in H_{\Gamma}^1(\Omega)$.

For the moment we work with a general $J(\cdot)$ which is assumed to be linear. We write the error in the quantity of interest relative to the computed solution u_n as:

$$J(u - u_n) = J(u) - J(u_n).$$

Then using the definition of the dual problem (15) and (14) we have

$$J(u - u_n) = F_c(z) - A(u_n, z).$$

This shows that the error in the quantity of interest is equal to the residual $F_c(z) - A(u_n, z)$ of the discrete primal problem. This result holds for any definition of the functional $J(\cdot)$ to which a different true dual solution z corresponds and so a different residual.

The residual $F_c(z) - A(u_n, z)$ is not computable in practice because it involves the true dual solution z . What is possible to do is to substitute z with a DG approximation z_n . Then, if z_n is a ‘‘good’’ approximation of z we have that

$$F_c(z) - A(u_n, z) \approx F_c(z_n) - A_n(u_n, z_n),$$

and consequently

$$J(u - u_n) \approx F_c(z_n) - A_n(u_n, z_n).$$

In order to use this error estimator, due to the fact that $F(v_n) - A_n(u_n, v_n) = 0$ for all $v_n \in S_n$, it is necessary to compute z_n in a DG space finer than S_n . In all our experiments we see that increasing by 1 the polynomial degree in all elements of the finite element space S_n , which was used to compute u_n , is enough to guarantee that z_n is a “good” approximation of z . Furthermore, the residual $F(z_n) - A_n(u_n, z_n)$ can be split in elementwise contributions $\tilde{\eta}_K$ and so the DWR a posteriori error estimator can be defined as:

$$\tilde{\eta} := \sum_{K \in \mathcal{T}_n} \tilde{\eta}_K ,$$

which satisfies

$$J(u - u_n) \approx \tilde{\eta} . \quad (16)$$

So (16) implies that the value $\tilde{\eta}$ is very close to the measurement of the error $J(u - u_n)$ of interest and it is computable also when the true solutions u and z are unknown. Also using the DWR a posteriori error estimator $\tilde{\eta}$, it is possible to construct a sequence of meshes automatically designed to minimize the measurement of the error of interest.

Moreover, the error estimator $\tilde{\eta}$ can be also used to compute an enhanced approximation of the quantity of interest $J(u)$ applying the formula:

$$J(u) \approx J(u_n) + \tilde{\eta} . \quad (17)$$

5 Adaptivity

The hp -adaptive algorithm used for the numerical experiments in Section 6 is expressed below in Algorithm 1.

Algorithm 1 Adaptive algorithm

```

 $(u_n, \mathcal{T}_n, S_n) := \text{AdaptDG}(\mathcal{T}_1, S_1, \theta, \text{tol})$ 
 $n = 1$ 
repeat
  Compute the solution  $u_n$  on  $\mathcal{T}_n$ 
  Compute  $\eta_K$  for all  $K \in \mathcal{T}_n$ 
  if  $\sum_{K \in \mathcal{T}_n} \eta_K^2 < \text{tol}^2$  then
    exit
  else
     $(\mathcal{T}_{n+1}, S_{n+1}) := \text{Refine}(\mathcal{T}_n, S_n, \theta, \eta)$ 
     $n = n + 1$ 
  end if
until

```

This algorithm takes as input: an initial mesh \mathcal{T}_1 , an initial DG space S_1 , a real value $0 \leq \theta \leq 1$ to tune the marking strategy, a real and positive value tol which prescribes the required tolerance. The function `Refine` applies a simple fixed-fraction strategy to mark a minimal subset of elements containing

a portion of the error proportional to θ . Then the choice for each marked element between splitting the element into smaller elements (h -refinement) or increasing the polynomial order (p -refinement) is made by testing the local analyticity of the computed solution in the interior of the element as described in [25,26]. In the case that we are only interested in using h -refinement the local analyticity test can be avoided. When the DWR error estimator is used, the residuals $\tilde{\eta}_K$ are computed instead of η_K .

6 Numerical experiments

In this section we present five examples. For all examples we show the convergence of the error.

6.1 Acoustic cavity problem

The first problem which we examine comes from [27] and it is posed on a rectangular domain of measurements 2×1 :

$$\begin{cases} -\Delta u - (\omega/c)^2 u = 0 & \text{in } \Omega, \\ u = p & \text{on } \partial\Omega, \end{cases} \quad (18)$$

this problem has no source term and inhomogeneous Dirichlet boundary conditions everywhere on the boundary $\partial\Omega$. For this problem the frequency $\omega = 30000$, the speed of sound is $c = 331.3$. Also the solution u of (18) is known analytically in this case:

$$u(x, y) = ic \left(\frac{\cos(2\omega/c)}{\sin(2\omega/c)} \cos(\omega/c x) + \sin(\omega/c x) \right).$$

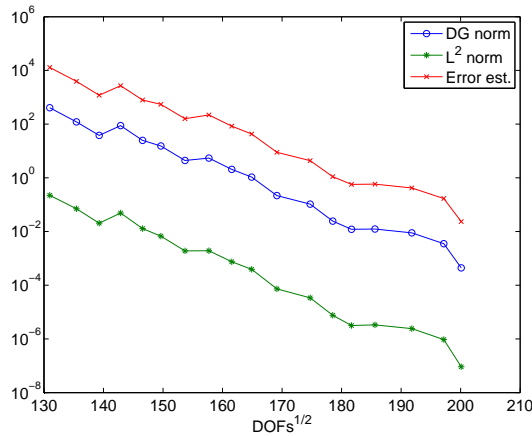


Fig. 1 Convergence of the error in the L^2 and DG norm and convergence of the error estimator expressed in degrees of freedom (DOFs).

In Figure 1 we plot the convergence curves for the DG norm, the L^2 norm and the error estimator η related to a sequence of adaptively refined meshes generated using our hp -adaptive algorithm. As can be seen all curves reassemble straight lines which suggests exponential convergence rates.

6.2 Green function in a box

For our second example we consider the problem:

$$\begin{cases} -\Delta u - (\omega/c)^2 u = \delta_s & \text{in } \Omega, \\ u = G_{s,\omega} & \text{on } \partial\Omega, \end{cases}$$

where $\Omega = [0, 1]^2$, the frequency $\omega = 30000$, δ_s is the delta of Dirac distribution centered in $s = (0.51, 0.51) \in \Omega$ and $G_{s,\omega}$ is the Green function centered in s and for frequency ω . So, it is clear from the setup of the problem that the true solution is $u = G_{s,\omega}$. Also in this case we used the error estimator η .

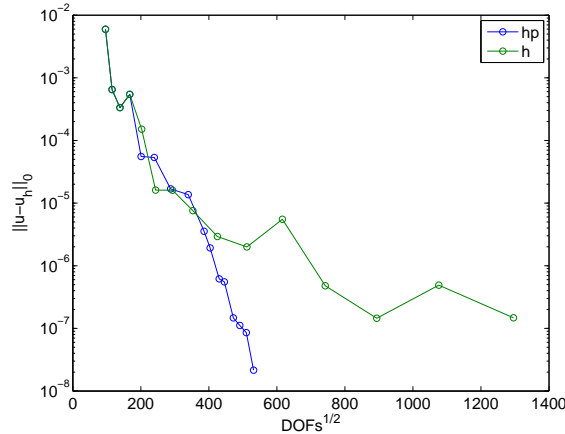


Fig. 2 Convergence in the L^2 norm for the h - and hp -adaptive method.

In Figure 2 we plot the convergence curves for the L^2 norm using either h - or hp -adaptivity, as can be seen the the gap between the two is quite remarkable. The plot seems to suggests that the hp -adaptive method converges exponentially.

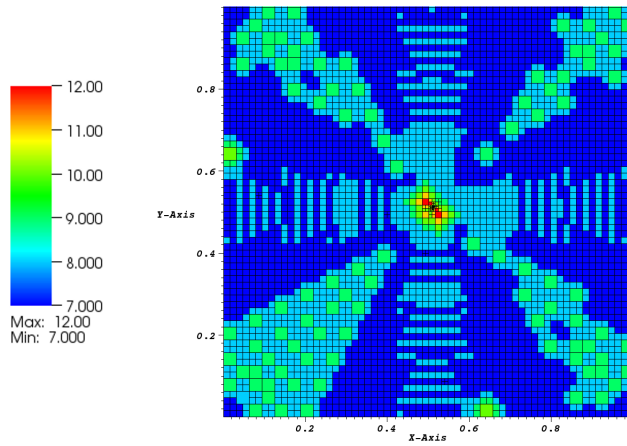


Fig. 3 Adapted mesh after 16 iterations.

In Figure 3 we plot the mesh generated after 16 iterations by the hp -adaptive method. As can be seen the mesh is particularly refined around the position of the source which indicates that the method automatically recognizes a lack of regularity due to the pointwise source.

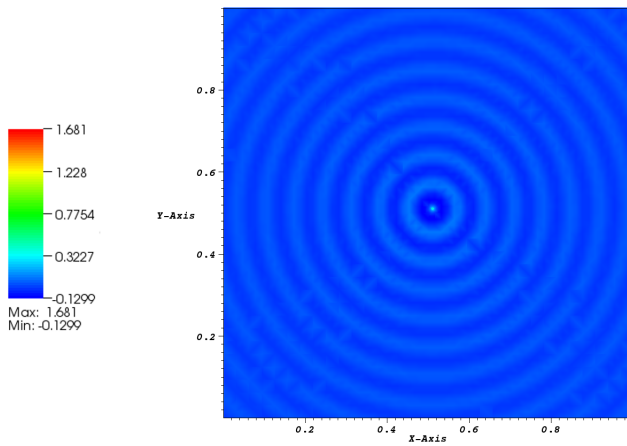


Fig. 4 Solution.

In Figure 4 we plot the computed solution.

6.3 Green function in a box with goal-oriented adaptivity

For our third example we consider the same problem as in the previous example. But in this example we use the goal-oriented error estimator $\tilde{\eta}$ with point of interest $r = (0.21, 0.21)$, so in this example the error estimator drives the adaptive procedure to minimize the error at the point r .

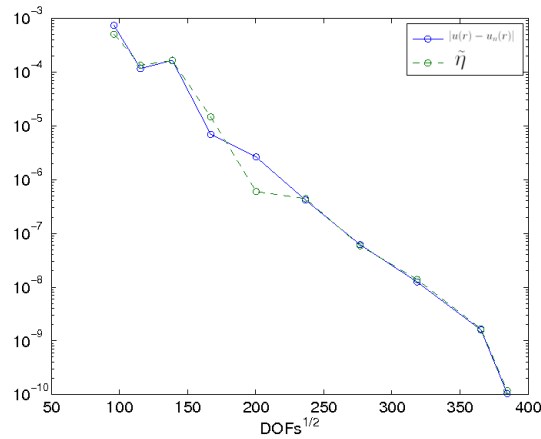


Fig. 5 Convergence of the error and of the error estimator in degrees of freedom (DOFs) versus the error at r .

In Figure 5 we plot the convergence curves for the true error $|u(r) - u_n(r)|$ and for the estimator $\tilde{\eta}$. The fact that the curves look like straight lines, suggests exponential convergence also for this example. Comparing these results with Figure 1, it is clear that the error estimator $\tilde{\eta}$ is sharper than η because there is almost no gap between the estimated values of the error and the true error.

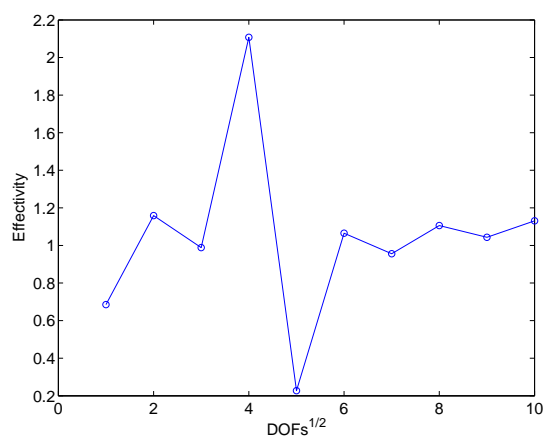


Fig. 6 Effectivity of the error estimator $\tilde{\eta}$ with hp -adaptivity.

In Figure 6 we plot the effectivity index computed using the formula $|\tilde{\eta}|/|J(u) - J(u_n)|$. As can be seen the index is almost everywhere very close to 1 which implies that the error estimator is sharp in respect to the true error. The effectivity index for the DWR error estimator can also be interpreted as a way to check if the dual finite element space is fine enough compared to S_n . When the dual finite element space is fine enough, the effectivity index is close to 1, when it is not fine enough, the effectivity index is far from 1.

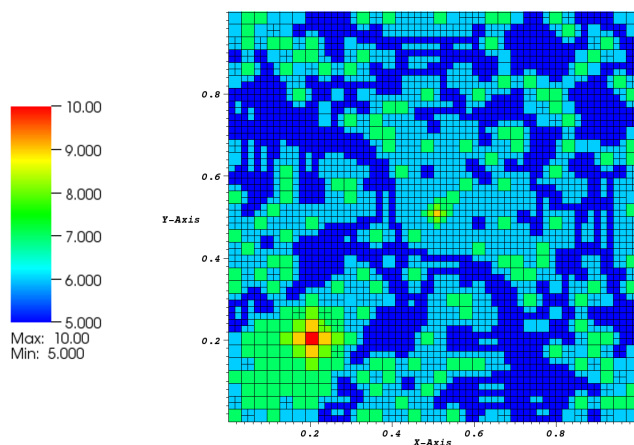


Fig. 7 Adapted mesh after 10 iterations.

In Figure 7 we plot the mesh generated after 10 iterations by the hp -adaptive method. Comparing it with Figure 3 it is clear that the two error estimators work very differently. In order to reduce the norm of the error, the error estimator η refines quite heavily around the source. Instead in order to reduce the error at the point of interest, the error estimator $\tilde{\eta}$ refines more around r .

6.4 Complex Green function in a box with goal-oriented adaptivity

For our fourth example we consider the problem:

$$\begin{cases} -\Delta u - (\omega/c)^2 u = \delta_s & \text{in } \Omega, \\ u = G_{s,\omega} & \text{on } \partial\Omega, \end{cases}$$

where $\Omega = [0, 1]^2$, the frequency $\omega = 6000 + i66.26$, δ_s is the delta of Dirac distribution centered in $s = (0.51, 0.51) \in \Omega$. Because ω has an imaginary part different from zero, we have damping in this example.

Also in this example we use the goal-oriented error estimator $\tilde{\eta}$ with point of interest $r = (0.21, 0.21)$.

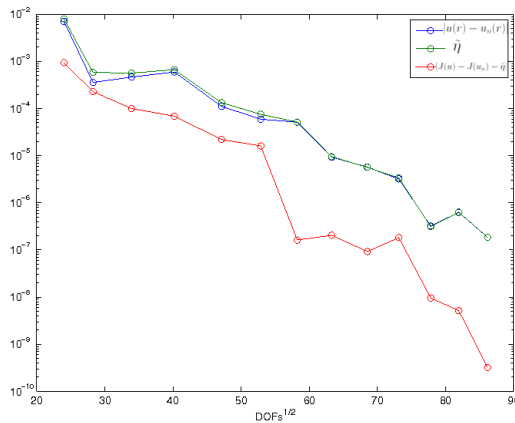


Fig. 8 Convergence rate expressed in degrees of freedom (DOFs) versus the error at r .

In Figure 8 we plot the convergence curves for the true error $|u(r) - u_n(r)|$ and for the estimator $\tilde{\eta}$. The red curve is the error relative to the enhanced estimation (17), as can be seen the improvement is about of at least one order. The fact that the curves look like straight lines, suggests exponential convergence also for this example.

6.5 Two plates problem with different materials

For our last example we consider the problem:

$$\begin{cases} -\nabla \cdot (\mathcal{A}\nabla u) - (\omega/c)^2 u = \delta_s \text{ in } \Omega, \\ u = 0 \text{ on } \partial\Omega, \end{cases}$$

where Ω is formed by two polygonal plates (see Figure 10), the frequency $\omega = 30000$, δ_s is the delta of Dirac distribution centered in $s = (-0.4, 0.5) \in \Omega$ and \mathcal{A} is equal to 1 on the left plate and 2 on the right plate.

In this example we use the goal-oriented error estimator $\tilde{\eta}$ with point of interest $r = (0.51, 0.51)$.

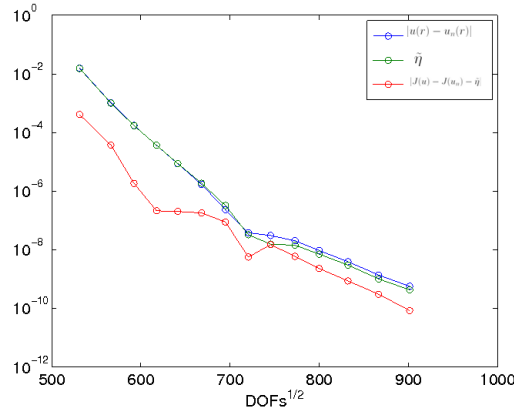


Fig. 9 Convergence rate expressed in degrees of freedom (DOFs) versus the error at r .

In Figure 9 we plot the convergence curves for the true error $|u(r) - u_n(r)|$, for the estimator $\tilde{\eta}$ and for the improved estimation in (17). The fact that the curves look like straight lines, suggests exponential convergence also for this example.

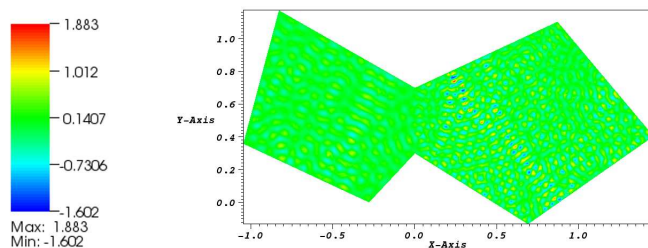


Fig. 10 solution.

In Figure 10 we plot the computed solution. As can be seen the different materials have a clear effect on the wave length.

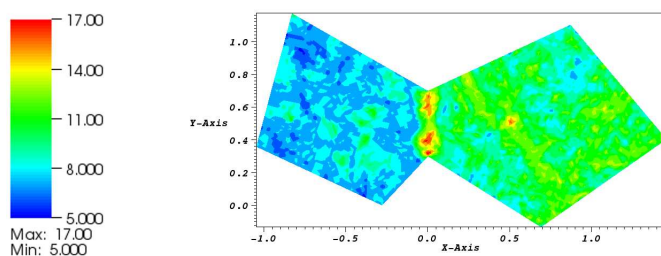


Fig. 11 Order of polynomials for the adapted mesh.

In Figure 11 we plot the distribution of the different orders of polynomials. Clearly the two regions mostly refined are the location of the point of interest r and the interface between the two plates where the material changes.

References

1. N. Lalor and H.-H. Priebsch. The prediction of low- and mid-frequency internal road vehicle noise: a literature survey. *Proceedings of the Institution of Mechanical Engineers, Part D: Journal of Automobile Engineering*, 221(3):245–269, 2007.
2. B. van Hal, H. Hepberger, H.-H. Priebsch, W. Desmet, and P. Sas. High performance implementation and conceptual development of the wave based method for steady-state dynamic analysis of acoustic problems. Technical report.
3. B. Pluymers, Wim Desmet, D. Vandepitte, and P. Sas. Wave based modelling methods for steady-state interior acoustics: an overview. Technical report.

4. H. Hepberger, H.-H. Priebsch, Wim Desmet, B. van Hal, B. Pluymers, and P. Sas. Application of the wave based method for the steady-state acoustic response prediction of a car cavity in the mid-frequency range. Technical report.
5. J. Rejlek, F. Diwojky, H. Hepberger, and B. Pluymers. Wave based technique: enrichment of the set of basis functions. Technical report.
6. J. Rejlek, B. Pluymers, F. Diwojky, H. Hepberger, H.-H. Priebsch, and W. Desmet. Validation of the wave based technique for the analysis of 2D steady-state acoustic radiation problems. Technical report.
7. A. Moiola, R. Hiptmair, and I. Perugia. Plane wave approximation of homogeneous helmholtz solutions. *Zeitschrift fr Angewandte Mathematik und Physik (ZAMP)*, 62(5):809–837, 2011.
8. G. Tanner. Dynamical energy analysis—determining wave energy distributions in vibro-acoustical structures in the high-frequency regime. *Journal of Sound and Vibration*, 320(4-5):1023–1038, 2009.
9. D. Chappell, S. Giani, and G. Tanner. Dynamical energy analysis for built-up acoustic systems at high frequencies. *JASA*, 130(3):1420–1429, 2011.
10. D.J. Chappell, G. Tanner, and S. Giani. Boundary element dynamical energy analysis: a versatile method for solving two or three dimensional wave problems in the high frequency limit. *Journal of Computational Physics*, 231(18):6181–6191, 2012.
11. J. Biermann, O. von Estorff, S. Petersen, and C. Wenterodt. Higher order finite and infinite elements for the solution of helmholtz problems. *Computer Methods in Applied Mechanics and Engineering*, 198(13-14):1171–1188, 2009.
12. Ph. Bouillard and F. Ihlenburg. Error estimation and adaptivity for the finite element method in acoustics: 2D and 3D applications. *Computer Methods in Applied Mechanics and Engineering*, 176(1-4):147–163, 1999.
13. C. Farhat, R. Tezaur, and P. WeidemannGoiran. Higherorder extensions of a discontinuous Galerkin method for midfrequency helmholtz problems. *International Journal for Numerical Methods in Engineering*, 61(11):1938–1956, 2004.
14. C. Farhat, R. Tezaur, and J. Toivanen. A domain decomposition method for discontinuous Galerkin discretizations of helmholtz problems with plane waves and lagrange multipliers. *International Journal for Numerical Methods in Engineering*, 78(13):1513–1531, 2009.
15. C. Farhat, I. Harari, and U. Hetmaniuk. A discontinuous Galerkin method with lagrange multipliers for the solution of helmholtz problems in the mid-frequency regime. *Computer Methods in Applied Mechanics and Engineering*, 192(11-12):1389–1419, 2003.
16. R. Hiptmair, A. Moiola, and I. Perugia. Plane wave discontinuous Galerkin methods for the 2D helmholtz equation: Analysis of the p-version. *SIAM Journal on Numerical Analysis*, 49(1):264, 2011.
17. A. Ern, A. F. Stephansen, and P. Zunino. A discontinuous Galerkin method with weighted averages for advection-diffusion equations with locally small and anisotropic diffusivity. *IMA J. Numer. Anal.*, 29(2):235–256, 2009.
18. D. N. Arnold, F. Brezzi, B. Cockburn, and L. D. Marini. Unified analysis of discontinuous Galerkin methods for elliptic problems. *SIAM J. Numer. Anal.*, 39(5):1749–1779, 2001.
19. P. Houston, D. Schötzau, and T. P. Wihler. Energy norm a posteriori error estimation of hp-adaptive discontinuous Galerkin methods for elliptic problems. 17(1):33–62, 2007.
20. R. Becker and R. Rannacher. An optimal control approach to a posteriori error estimation in finite element methods. *Acta Numer.*, 10:1–102, 2001.
21. V. Heuveline and R. Rannacher. A posteriori error control for finite approximations of elliptic eigenvalue problems. *Adv. Comput. Math.*, 15(1-4):107–138, 2001.
22. S. Giani and P. Houston. Anisotropic hp-adaptive discontinuous Galerkin finite element methods for compressible fluid flows. *International Journal of Numerical Analysis and Modeling*, 9(4):928–940, 2012.
23. S. Giani, L. Grubišić, and J. S. Owall. Benchmark results for testing adaptive finite element eigenvalue procedures. *Applied Numerical Mathematics*, 62(2):121–140, 2012.
24. A. Cliffe, E. Hall, P. Houston, E. T. Phipps, and A. G. Salinger. Adaptivity and a posteriori error control for bifurcation problems II: Incompressible fluid flow in open systems with z_2 symmetry. *Journal of Scientific Computing*, 47(3):389–418, 2011.

25. T. Eibner and J. M. Melenk. An adaptive strategy for hp-FEM based on testing for analyticity. *Computational Mechanics*, 39(5):575–595, 2006.
26. P. Houston and E. Süli. A note on the design of hp-adaptive finite element methods for elliptic partial differential equations. *Computer Methods in Applied Mechanics and Engineering*, 194(2-5):229–243, 2005.
27. A. Hepberger, H.-H. Priebsch, W. Desmet, B. van Hal, B. Pluymers, and P. Sas. Application of the wave based method for the steady-state acoustic response prediction of a car cavity in the mid-frequency range. Technical report.
28. W. Reed and T. Hill. Triangular mesh methods for the neutron transport equation. Technical report, Los Alamos Scientific Laboratory, 1973.
29. L. Zhu and D. Schötzau. A robust a-posteriori error estimate for hp-adaptive DG methods for convection-diffusion equations. *IMA J. Numer. Anal.*, 31:971–1005, 2011.
30. L. Zhu, S. Giani, D. Schötzau, and P. Houston. Energy norm a-posteriori error estimation for hp-adaptive discontinuous Galerkin methods for elliptic problems in three dimensions. *Math. Models Methods Appl. Sci.*, 2009.
31. B. Cockburn. Discontinuous Galerkin methods for convection-dominated problems. in high-order methods for computational physics. volume 9 of *Lect. Notes Comput. Sci. Eng.*, pages 69–224. Springer, Berlin, 1999.
32. B. Cockburn, G. E. Karniadakis, and C. W. Shu. The development of discontinuous Galerkin methods. in discontinuous Galerkin methods. volume 11 of *Lect. Notes Comput. Sci. Eng.*, pages 3–50. Springer, Berlin, 2000.
33. P. Houston, C. Schwab, and E. Süli. Discontinuous hp-finite element methods for advection-diffusion-reaction problems. *SIAM J. Numer. Anal.*, 39(6):2133–2163, 2002.
34. P. Houston and E. Süli. hp-adaptive discontinuous Galerkin finite element methods for first-order hyperbolic problems. *SIAM J. Sci. Comput.*, 23(4):1226–1252, 2001.
35. F. Brezzi, L. D. Marini, and E. Süli. Discontinuous Galerkin methods for first-order hyperbolic problems. *Math. Models Methods Appl. Sci.*, 14(12):1893–1903, 2004.
36. R. Hartmann and P. Houston. Error estimation and adaptive mesh refinement for aerodynamic flows. In H. Deconinck, editor, *VKI LS 2010-01: 36th CFD/ADIGMA course on hp-adaptive and hp-multigrid methods, Oct. 26-30, 2009*. Von Karman Institute for Fluid Dynamics, Rhode Saint Genèse, Belgium, 2009.
37. P. Houston, C. Schwab, and E. Süli. Discontinuous hp-finite element methods for advection-diffusion-reaction problems. *SIAM J. Numer. Anal.*, 39(6):2133–2163, 2002.
38. P. Houston, D. Schötzau, and T. P. Wihler. Energy norm a posteriori error estimation of hp-adaptive discontinuous Galerkin methods for elliptic problems. *Math. Mod. Meth. Appl. Sci.*, 17(1):33–62, 2007.
39. T. Leicht and R. Hartmann. Error estimation and hp-adaptive mesh refinement for discontinuous Galerkin methods. In Zhi J. Wang, editor, *Adaptive High-Order Methods in Computational Fluid Dynamics*, volume 2, chapter 3 of *Advances in Computational Fluid Dynamics*, pages 67–94. World Science Books, 2011.
40. I.M. Babuska and S. A. Sauter. Is the pollution effect of the FEM avoidable for the helmholtz equation considering high wave numbers? *SIAM Review*, 42(3):451–484, 2000.
41. O. Cessenat and B. Despres. Application of an ultra weak variational formulation of elliptic PDES to the two-dimensional helmholtz problem. *SIAM Journal on Numerical Analysis*, 35(1):255–299, 1998.
42. O. Hüseyin. High-order discontinuous Galerkin method on hexahedral elements for aeroacoustics. Technical report.
43. O. Laghrouche, P. Bettess, and R. J. Astley. Modelling of short wave diffraction problems using approximating systems of plane waves. *International Journal for Numerical Methods in Engineering*, 54(10):1501–1533, 2002.
44. E. Perrey-Debain, O. Laghrouche, P. Bettess, and J. Trevelyan. Plane-wave basis finite elements and boundary elements for three-dimensional wave scattering. *Philosophical Transactions of the Royal Society A: Mathematical, Physical and Engineering Sciences*, 362:561–577, 2004.
45. B. Pluymers. Wave based modelling methods for steady-state vibro-acoustics. Technical report.
46. B. Pluymers, B. van Genechten, P. Silar, H. Hepberger, and W. Desmet. Validation of a direct/indirect hybrid finite element - wave based method for 3D steady-state acoustic analysis. Technical report.

-
47. Y. Reymen, W. De, R. G. Rubio, M. Baelmans, and W. Desmet. A 3D discontinuous Galerkin method for acoustic propagation in duct flows.
 48. P. Silar, H. Hepberger, H.-H. Priebsch, H. Pramberger, and T. Bartosch. Direct hybrid coupled finite element wave based technique for 3D steady-state acoustic analysis. Technical report.
 49. G. Tanner and N. Søndergaard. Wave chaos in acoustics and elasticity. *Journal of Physics A: Mathematical and Theoretical*, 40(50):R443–R509, 2007.
 50. M. Petzoldt. A posteriori error estimators for elliptic equations with discontinuous coefficients. *Adv. Comput. Math.*, 16(1):47–75, 2002.